

Production of O₂ Herzberg states in the deep UV photodissociation of ozone

R. Schinke,^{1,a)} G. C. McBane,^{2,b)} L. Shen,³ P. C. Singh,³ and A. G. Suits^{3,c)}

¹Max-Planck-Institut für Dynamik und Selbstorganisation, D-37073 Göttingen, Germany

²Department of Chemistry, Grand Valley State University, Allendale, Michigan 49401, USA

³Department of Chemistry, Wayne State University, Detroit, Michigan 48202, USA

(Received 21 April 2009; accepted 30 May 2009; published online 6 July 2009)

High-resolution imaging experiments combined with new electronic structure and dynamics calculations strongly indicate that the O(³P)+O₂ products with very low kinetic energy release ($E_{tr} < 0.2$ eV) formed in the deep UV (226 nm) photodissociation of ozone reflect excitation of the Herzberg states of O₂: A' ³Δ_u($v=0, 1, 2$) and A ³Σ_u⁺($v=0, 1$). This interpretation contradicts the earlier assignment to very high ($v \geq 26$) vibrational states of O₂(³Σ_g⁻). © 2009 American Institute of Physics. [DOI: 10.1063/1.3157236]

The strong Huggins/Hartley band system of ozone (200 nm < λ < 350 nm) is due to excitation of the third state with ¹A' symmetry (¹B₂ in C_{2v}), termed *B* in what follows.^{1,2} The *B* state correlates diabatically with the singlet channel (2), O(¹D)+O₂(¹Δ_g), with a quantum yield of the order of 90%;¹ the remaining quantum yield is mainly associated with the triplet channel (1), O(³P_{*j*})+O₂(³Σ_g⁻), accessed by a transition to a repulsive state *R* with the same ¹A' symmetry.³

The maximum excess energy released in the triplet channel ranges from 3.6 eV at 266 nm to 4.4 eV for dissociation at 226 nm. Several research groups have measured the partitioning of the available energy between translation (E_{tr}) and O₂ internal energy by imaging the O(³P_{*j*}) product at several dissociation wavelengths.^{1,4–10} All distributions $P(E_{tr})$ have a broad maximum of around 2 eV corresponding to vibrational states of $v \approx 10–15$ of O₂(³Σ_g⁻). Classical trajectory surface hopping (TSH)^{3,11} calculations unambiguously attribute this main part to the *B* → *R* transition.

At all wavelengths, $P(E_{tr})$ extends to very low energies. For longer wavelengths the shape of the low-energy part varies gradually with λ.⁹ However, at 233 nm, there is a qualitative change: a very sharp peak near $E_{tr} \approx 0$, several times higher than the main peak, suddenly appears out of the broad low-energy part of the distribution. At shorter wavelengths this new peak broadens but remains distinct from the slowly varying component. It may be attributed to excitation of either very high vibrational states $v \geq 26$ in channel (1) or to the excited triplet (Herzberg) states (3) O(³P_{*j*})+O₂(A' ³Δ_u) and (3') O(³P_{*j*})+O₂(A ³Σ_u⁺), which open at 234.1 nm.¹²

In this communication we present new imaging experiments and new electronic structure and dynamics calculations that provide strong evidence that the low- E_{tr} peak corresponds to the excited triplet channels (3) and (3') rather than channel (1). The broad low-energy part of $P(E_{tr})$ found

at all wavelengths is not part of this study and remains unexplained.

The experiments were performed using dc slice imaging¹³ in an apparatus described previously. Ozone was trapped onto silica gel in a dry ice bath. Argon at 2 bar was flowed over the silica gel into a pulsed valve. The silica gel was held in the dry ice bath during the experiment to produce a very dilute beam. The ozone beam passed through a skimmer and then crossed two laser beams each tuned 10 cm⁻¹ on opposite sides of the oxygen atom 2+1 ionization resonance, 44 315 cm⁻¹ for O(³P₂) and 44 237 cm⁻¹ for O(³P₁). The laser beams achieved both single photon dissociation of ozone and two-color reduced Doppler detection¹⁴ of the O(³P_{*j*}) product. The dissociation/ionization took place in a velocity map imaging^{15,16} electrode assembly optimized for high resolution slice imaging (4 electrodes, repeller of -350 V). The resulting ions were accelerated down a 1.2 m flight tube onto a 120 mm imaging detector. Higher energy products were allowed to fly out of the detection window because our interest in this study was exclusively the very slow channel. The images were analyzed to give $P(E_{tr})$ using our in-house suite of programs.¹⁷ Calibration of E_{tr} was performed using both O₂ dissociative ionization at 225 nm (Ref. 15) and OCS photodissociation to give CO($j=65$) at 230 nm.¹⁸ These alternative methods gave results that agreed within 5%. The resolution in the experiment was ultimately limited by the O⁺ recoil in the resonantly enhanced multiphoton ionization step, which contributes up to 35 m/s uncertainty in the measured O atom velocity.¹⁷

The measured distributions of kinetic energies for O(³P₁) and O(³P₂), shown along with the sliced images in Fig. 1 have two prominent peaks at low E_{tr} and a smaller featureless background extending to higher energies. They agree very well with the earlier observations^{9,10} at the same λ, although the new data have better energy resolution. The threshold energies for the possible electronic and vibrational states of O₂ were calculated with 1.0523 eV for the O₃ → O(³P₂)+O₂(³Σ_g⁻) dissociation energy,¹ 158.3 cm⁻¹ for the O(³P₂)-O(³P₁) splitting, the vibrational energies (G_v) of

^{a)}Electronic mail: rschink@gwdg.de.

^{b)}Electronic mail: mcbaneg@gvsu.edu.

^{c)}Electronic mail: asuits@chem.wayne.edu.

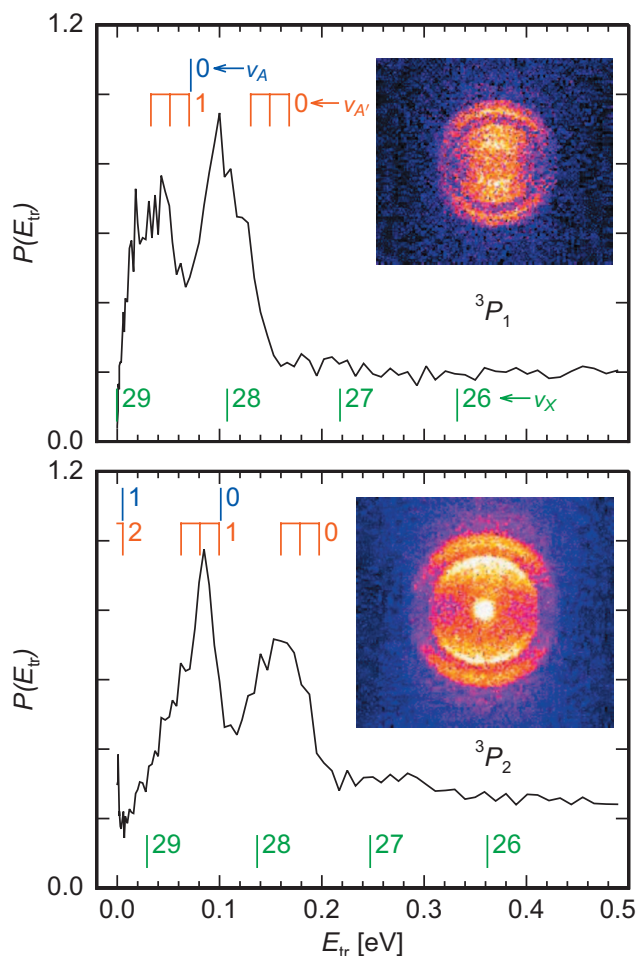


FIG. 1. Sliced ion images and measured distributions $P(E_{tr})$ for $O(^3P_1)$ (upper panel) and $P(E_{tr})$ for $O(^3P_2)$ (lower panel). These distributions are separately normalized. The threshold energies for the possible dissociation channels are indicated by the vertical lines: (1) $O(^3P) + O_2(^3\Sigma_g^-, v_x)$ (green); (3) $O(^3P) + O_2(^3\Delta_u, v_{A'})$ (red); (3') $O(^3P) + O_2(^3\Sigma_u^+, v_A)$ (blue). The three energies for channel (3) represent the three spin states Ω of $O_2(^3\Delta_u)$.

Jongma *et al.*¹⁹ for $O_2(^3\Sigma_g^-)$, and the G_v values given by Slanger and Cosby¹² for $O_2(A' ^3\Delta_u; \Omega)$ and $O_2(A ^3\Sigma_u^+; \Omega = 1-3)$ denotes the three spin-orbit states of $O_2(^3\Delta_u)$.

The high-energy edges of the faster peaks coincide within ~ 0.01 eV with the expected thresholds for production of $v=0$ and $\Omega=3$ of channel (3). The edges of the slower peaks agree similarly well with the $v=1$ threshold for channel (3) and the $v=0$ threshold of channel (3'), which are nearly degenerate. For 3P_2 , $P(E_{tr})$ exhibits a very narrow peak very close to zero that reflects the bright spot in the center of the sliced image. It may be attributed to $v=2$ and $\Omega=3$ of channel (3) and/or $v=1$ of channel (3'), which are both barely open (0.005 eV). No similar peak appears for $O(^3P_1)$. The shapes of the observed peaks are consistent with excitation of all three spin components of $^3\Delta_u$: $\Omega=3, 2,$ and 1 (in order of increasing energy). The population of the Ω states depends on both J and v . The shift of about 0.01–0.02 eV to lower energies with respect to the threshold energies is in accordance with modest rotational excitation of the O_2 product. The observed peaks do not have an obvious relation to the thresholds for production of vibrationally excited $O_2(X ^3\Sigma_g^-)$.

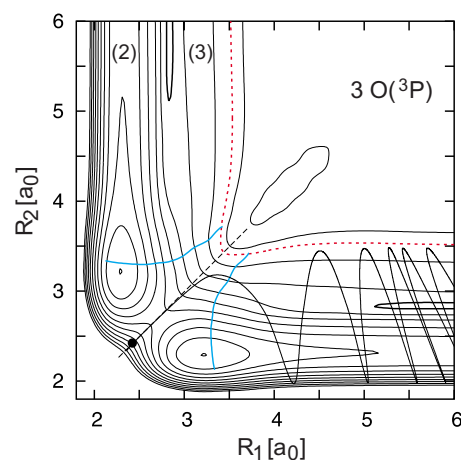


FIG. 2. Two-dimensional representation of the diabatic B -state PES for $\alpha = 100^\circ$. The highest contour is $E=6$ eV and $\Delta E=0.25$ eV with $E=0$ corresponding to the equilibrium of the ground state X . The heavy dot marks the FC point and the dotted line (online: red) indicates the contour $E=5.66$ eV corresponding to $\lambda=226$ nm. The two thick contour lines ($E=5.25$ eV) emphasize the barrier between channels (2) and (3) and the two bent lines (online: blue) represent the B/R crossing. A typical trajectory ($E=5.66$ eV) with small translational and large vibrational energy is displayed.

Understanding the path leading to excitation of the Herzberg states requires knowledge on excited electronic states of ozone and the changes in electronic structure from the Franck–Condon (FC) region out to the products. Here we use a global diabatic potential energy surface (PES) for the B state (V_B , Fig. 2),² determined by multireference configuration interaction (MRCI) calculations (including Davidson correction) with the augmented correlation consistent triple-zeta basis.¹¹ The lowest five states with $^1A'$ symmetry were calculated and diabatic PESs for four states $X, A, B,$ and R were constructed as described by Qu *et al.*²⁰ Five states are sufficient for describing channels (1) and (2). However, more states are required in order to explain the population of the Herzberg channels (3) and (3').

We call the O–O bond coordinate that eventually breaks R_1 , and the bond that remains, the O_2 stretching coordinate, R_2 . Most trajectories that start on V_B near the FC region²¹ very quickly dissociate into the singlet channel (2). About one tenth of the trajectories in the vicinity of the B/R crossing seam “hop” to the repulsive R -state PES and dissociate to the triplet channel (1), yielding the highly inverted vibrational distribution of $O_2(^3\Sigma_g^-)$ seen in all experiments.¹ Calculations describe the main part of this distribution very well.^{3,11} However, the calculated $P(E_{tr})$ for this pathway at 226 nm is practically zero below 0.8 eV.

Far in the exit channel ($R_1 \gtrsim 4.5a_0$) V_B has the shape of a double-well potential along the O_2 stretching coordinate. The deeper well at $R_2=2.3a_0$ belongs to the singlet channel (2) while the comparatively flat well around $2.8-2.9a_0$ results from the excited triplet channels (3)/(3'); a low barrier separates the two wells. To elucidate the electronic structure in this region we performed MRCI calculations as described above, but including the lowest ten $^1A'$ states. Cuts along the O_2 bond for two O– O_2 separations R_1 are depicted in Fig. 3. [Potential cuts for additional R_1 involving 12 states calcu-

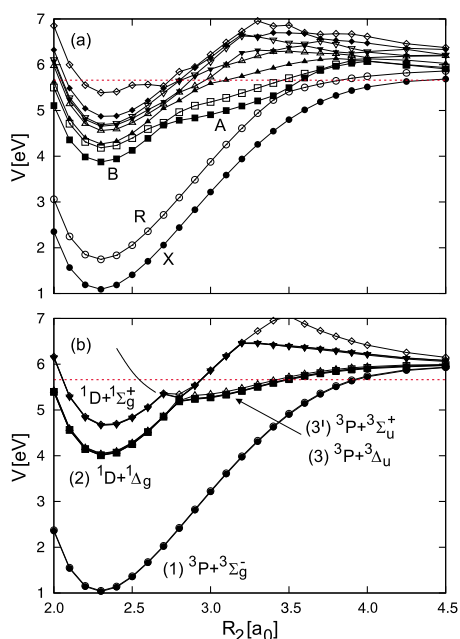


FIG. 3. Potential cuts along the O_2 stretching coordinate R_2 for (a) $R_1 = 4a_0$ and (b) $6a_0$ and $\alpha = 100^\circ$ as obtained from the CI calculations. X, A, B, and R in (a) label the diabatic states most important for the uv photodissociation. The dotted line (online: red) indicates the energy corresponding to $\lambda = 226$ nm. The extension of the Herzberg states to small R_2 (smooth solid line) is taken from CASSCF calculations.

lated at the complete active-space self-consistent field (CASSCF) level are available electronically.^{22]} Many of the states are nearly degenerate for $R_1 = 6a_0$ and the potential curves are those of free O_2 with O either in the ground or the excited state. The two states with minima around $R_2 \approx 2.9a_0$ are the Herzberg states $O_2(A' \ ^3\Delta_u)$ and $O_2(A \ ^3\Sigma_u^+)$ in combination with $O(^3P)$. The calculations predict a separation of ≈ 660 cm^{-1} in good agreement with the experimental value of 630 cm^{-1} .¹² The lowest Herzberg state $c \ ^1\Sigma_u^-$ correlates, in combination with $O(^3P)$, with the triplet states of ozone and therefore does not appear in Fig. 3. All potentials approach the $3O(^3P)$ three-body breakup limit for large R_2 .

The representation in Fig. 3(b) is misleading in that it suggests the possibility of transitions between the states belonging to channel (2) and those representing channels (3)/(3'). However, such transitions are impossible for infinitely separated O and O_2 because they would require an accompanying transition in the free atom. The “crossing” exists only because of the $^3P - ^1D$ excitation of the oxygen atom of 1.96 eV. The degeneracies are lifted with decreasing R_1 and the network of potentials becomes much more complex as illustrated for $R_1 = 4a_0$ in Fig. 3(a). The real crossings for infinite R_1 turn into a multitude of avoided crossings. All states have the same $^1A'$ symmetry and nonadiabatic transitions between them are, in principle, allowed.

The double-well behavior of V_B at large O– O_2 separations is due to the combination of channels (2) and (3) and in this sense it is an adiabatic PES. Truly diabatic PESs, which asymptotically correlate with either of the channels (2), (3), or (3'), are needed for accurate dynamics calculations. However, in view of the complexity of the potential curves in Fig. 3(a), especially in the region around $R_2 = 2.8a_0$, the construc-

tion of such diabatic PESs is currently impracticable. We can therefore describe the possible path leading to the Herzberg channels only with words and calculations on the single V_B surface rather than true multistate dynamics calculations.

A few percent of all trajectories started near the FC point on V_B with energy corresponding to 226 nm lead to products with extremely low translational energies ($\sim 4\%$ with $E_{tr} < 0.3$ eV). All these trajectories have one feature in common: they first perform an almost perfect symmetric stretch motion on the saddle and are driven to large O–O bond lengths (Fig. 2). From the first turning point they are deflected into the dissociation channel and finally perform wide-amplitude vibrational motion almost perpendicular to the dissociation path. The initial part of the trajectory is reminiscent of a classical periodic orbit.² The average rotational energy of the trajectories with very small E_{tr} is of the order of 0.01–0.02 eV.

Because V_B is an adiabatic PES, trajectories with large-amplitude vibration pass through the transition state (TS) region $R_2 \approx 2.8a_0$ and sample both product channels. In a quantitative multistate TSH calculation, however, the highly excited transient O_3 would decide at each crossing of the TS whether it stays in one channel or hops to another. The nonadiabatic couplings diminish with increasing R_1 , and beyond $R_1 \approx 5.5a_0$ or so transitions between channels (2) and (3)/(3') become unlikely and the populations are frozen. While O and O_2 separate, nonadiabatic transitions to state R are also possible. They could explain part of the nearly constant background in the measured $P(E_{tr})$ but not the distinct maxima below 0.2 eV. A quantitative evaluation of the populations of channels (3) and (3') is beyond our current capabilities. An estimation of the populations of the spin states $J=0-2$ and $\Omega=1-3$ is even more demanding and requires knowledge on the triplet and quintet states of O_3 correlating with the Herzberg states.

The essential step in the proposed dissociation path leading to products with very small E_{tr} is the large-amplitude symmetric stretching in the very first moments of motion in the B state. It immediately and directly results in highly excited O_2 products.

Houston reported that “highly-excited fragments begin to be observed near 234.5 nm.”¹ The threshold for forming $O_2(^3\Delta_u)$ is 234.1 nm. This coincidence of observed and expected thresholds, the sudden appearance of large low-energy peaks in $P(E_{tr})$ between 234 and 233 nm,⁹ and the excellent correlation between measured peak edges and predicted thresholds in the new high-resolution data of Fig. 1 provide convincing evidence for electronic rather than vibrational excitation of O_2 .

Miller *et al.*⁵ rejected this possibility mainly on the basis of laser-induced fluorescence (LIF) pump-probe experiments, which clearly detected $O_2(^3\Sigma_g^-)$ in high vibrational levels, $19 \leq v \leq 26$. The observed vibrational distribution had a minimum at $v=22$ and matched well with the observed kinetic energy distribution of $O(^3P)$ atoms. The LIF experiments were carried out in ~ 100 torr of nitrogen and most LIF data were collected at 2 μs after the photolysis pulse. Although Miller *et al.* performed timing experiments to ensure that the observed vibrational distribution was not appre-

ciably modified by collisions with N_2 , those experiments were not performed with enough time resolution to eliminate the possibility of rapid *electronic* quenching of the O_2 Herzberg states.²³ The vibrational distribution with a minimum at $v=22$ seen in the LIF experiments was probably the superposition of a distribution of nascent vibrationally excited $O_2(X^3\Sigma_g^-)$ that decreased with increasing v , arising from the main part of channel (1), and a distribution of product states from electronic quenching of the Herzberg states.

Our assignment of the low-energy peaks to production of the Herzberg states suggests two obvious experimental tests. The first is a direct detection of the electronically excited O_2 products in either a molecular beam or a static gas photodissociation experiment. The second is the observation of the kinetics of production of very high vibrational states in $O_2(X)$ after photodissociation of ozone in a bath of N_2 to confirm their production by quenching of the Herzberg states.

We conclude that three processes contribute to the observed distribution of $O(^3P)$ kinetic energies. The main process requires a transition from the ozone B state to the R state, yielding ground-state molecular oxygen, and produces the main peak in $P(E_{tr})$. The second is dissociation to the O_2 Herzberg states $A' ^3\Delta_u$ and $A ^3\Sigma_u^+$ producing the sharp spikes that appear at very low kinetic energies for photolysis wavelengths ≤ 233 nm. Finally, there is a third process that yields the low, broad distribution of slow O atoms at all wavelengths. That process remains unknown and merits further experimental and theoretical investigation.

The theoretical and experimental works were supported by the DFG and the NSF, respectively, under award No. CHE-0175300. R.S. and G.C.M. acknowledge the invaluable input from S. Yu. Grebenshchikov in suggesting that electronically excited O_2 may be the nascent product. The authors thank A. Wodtke and P. Houston for valuable discus-

sions and N. Herath for assistance with the experiment.

- ¹P. L. Houston, in *Modern Trends in Chemical Reaction Dynamics; Experiment and Theory (Part 2)*, Advanced Series in Physical Chemistry Vol. 14, edited by X. Yang and K. Liu (World Scientific, Singapore, 2004).
- ²S. Yu. Grebenshchikov, Z.-W. Qu, H. Zhu, and R. Schinke, *Phys. Chem. Chem. Phys.* **9**, 2044 (2007).
- ³Z.-W. Qu, H. Zhu, S. Yu. Grebenshchikov, and R. Schinke, *J. Chem. Phys.* **122**, 191102 (2005).
- ⁴T. Kinugawa, T. Sato, T. Arikawa, Y. Matsumi, and M. Kawasaki, *J. Chem. Phys.* **93**, 3289 (1990).
- ⁵R. L. Miller, A. G. Suits, P. L. Houston, R. Toumi, J. A. Mack, and A. M. Wodtke, *Science* **265**, 1831 (1994).
- ⁶J. A. Syage, *J. Phys. Chem.* **99**, 16530 (1995).
- ⁷D. Stranges, X. Yang, J. D. Chesko, and A. G. Suits, *J. Chem. Phys.* **102**, 6067 (1995).
- ⁸K. Takahashi, N. Taniguchi, Y. Matsumi, and M. Kawasaki, *Chem. Phys.* **231**, 171 (1998).
- ⁹J. D. Geiser, S. M. Dylewski, J. A. Mueller, R. J. Wilson, R. Toumi, and P. L. Houston, *J. Chem. Phys.* **112**, 1279 (2000).
- ¹⁰M. Brouard, A. Goman, S. J. Horrocks, A. J. Johnsen, F. Quadriani, and W.-H. Yuen, *J. Chem. Phys.* **127**, 144304 (2007).
- ¹¹R. Schinke, S. Yu. Grebenshchikov, and G. C. McBane (unpublished).
- ¹²T. G. Slanger and P. C. Cosby, *J. Phys. Chem.* **92**, 267 (1988).
- ¹³D. Townsend, M. P. Minitti, and A. G. Suits, *Rev. Sci. Instrum.* **74**, 2530 (2003).
- ¹⁴C. S. Huang, W. Li, M. H. Kim, and A. G. Suits, *J. Chem. Phys.* **125**, 121101 (2006).
- ¹⁵D. H. Parker and A. T. J. B. Eppink, *J. Chem. Phys.* **107**, 2357 (1997).
- ¹⁶D. W. Chandler and P. L. Houston, *J. Chem. Phys.* **87**, 1445 (1987).
- ¹⁷W. Li, S. D. Chambreau, S. A. Lahankar, and A. G. Suits, *Rev. Sci. Instrum.* **76**, 063106 (2005).
- ¹⁸B. D. Leskiw, M. H. Kim, G. E. Hall, and A. G. Suits, *Rev. Sci. Instrum.* **76**, 104101 (2005).
- ¹⁹R. T. Jongma, S. Shi, and A. M. Wodtke, *J. Chem. Phys.* **111**, 2588 (1999).
- ²⁰Z.-W. Qu, H. Zhu, S. Yu. Grebenshchikov, and R. Schinke, *J. Chem. Phys.* **123**, 074305 (2005).
- ²¹R. Schinke, *Photodissociation Dynamics* (Cambridge University Press, Cambridge, England, 1993).
- ²²See EPAPS supplementary material at <http://dx.doi.org/10.1063/1.3157236> for additional potential cuts.
- ²³A. M. Wodtke, private communication (2009).